EUROPEAN ORGANIZATION FOR NUCLEAR RESEARCH

CERN LIBRARIES, GENEVA

LHC/Note 192
SL Note 92-30 (BI)
PS/BD Note 92-03
17th June 1992

PRELIMINARY STUDIES ON A PROFILE MONITOR FOR THE LHC USING SYNCHROTRON RADIATION

J. Bosser, C. Bovet and R. Jung

Abstract

Using synchrotron radiation (SR), appears to be an elegant, non-destructive method for measuring the LHC p-beam transverse profiles.

However, taking into account that

a) proton beams are dealt with,
b) the energy range is rather large,
c) the beam dimensions are quite small,

non-negligible problems have to be solved.

The most attractive solution requires the installation of two additional short magnets in an odd-numbered straight section, where the optics should be locally modified to provide adequate beam sizes.

1. INTRODUCTION

The aim of this paper is to look at the possibilities offered by synchrotron radiation (SR) to design a p-beam transverse profile monitor.

A first proposal has been made [1] where three types of light sources are considered. They are the radiation emitted by

a) a normal bending dipole,
b) a short magnet,
c) the edge effect of a dipole field,

for which the radiated frequency spectrum mainly ranges from the UV down to the visible light.

Synchrotron radiation profile monitors are mainly used at high-energy lepton machines. With protons the emitted power is usually too small to be detected.

The next sections will cover the following:

i) An estimate of the actual image detectors' sensitivity and of the expected p-beam dimensions. The latter will, of course, depend on the betatron functions at the location of the light source, and on the p-beam energy.
ii) Computation of the emitted power for the three above-mentioned sources.
iii) Estimation of the diffraction spots, which will set a limit to the instrument precision.
iv) Implementation of SR focussing telescopes in the Large Hadron Collider (LHC) machine with some emphasis on the example of the 'short magnet' case.

2. DETECTOR SENSITIVITY, BEAM DIMENSIONS

2.1 Detector sensitivity

In Section 6 a brief estimate is given of the sensitivity which can be obtained from actual image detectors. It is based on the experience acquired with the LEP profile monitors [2].

Usually the image of the light source is formed at the input of the frequency shifter–amplifier (Fig. 1). The goal of the 'shifter–amplifier' is to convert and to amplify the light from the UV range, where diffraction is limited, to the visible range where image detectors are most sensitive.

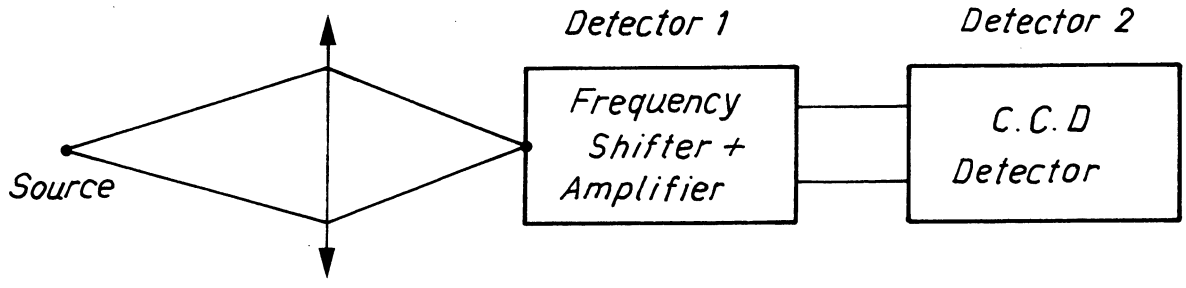

Figure 1

Principle of the detector layout

The Charge Coupled Device (CCD) operates in the visible range and offers a low noise level and a simple electronic treatment.

With this arrangement, an emitted power of 10^{-12} W or more can give significant measurements (Section 6) of the transverse profile.

2.2 Detectors' spectral response

a) The spectral response of detector 1 (or frequency shifter + amplifier) is given by Fig. 2. It has been approximated by

$$d_1 = \exp\left[-\frac{1}{2}\left(\frac{\lambda - \lambda_0}{\sigma_\lambda}\right)^2\right]$$

with $\lambda_0 = 240$ nm, $\sigma_\lambda = 55$ nm.

b) The spectral response of detector 2 (or the CCD detector) is given by Fig. 3. It has been approximated by

$$d_2 = \cos \Omega(\lambda - \lambda_0) \qquad \text{for } \lambda \in [340\text{ nm}, 1100\text{ nm}]$$

$$d_2 = 0 \qquad \text{for } \lambda \notin [340\text{ nm}, 1100\text{ nm}]$$

with $\Omega = 4.189 \times 10^6$, $\lambda_0 = 725$ nm.

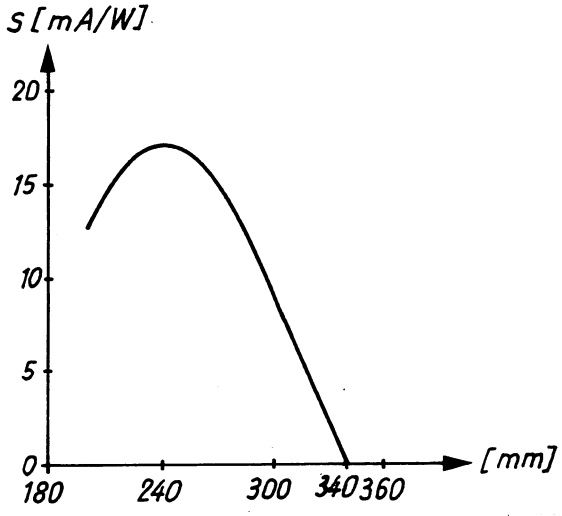

Figure 2
Spectral response of the frequency shifter–amplifier with solar-blind filter

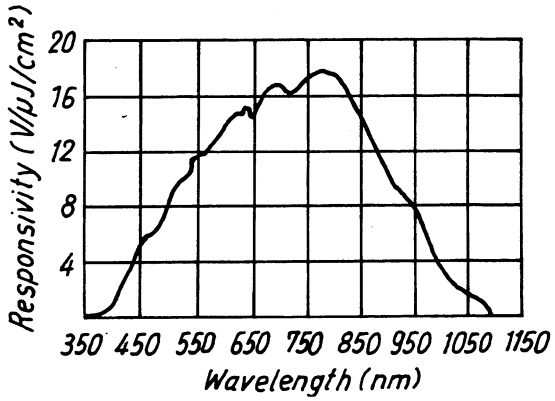

Figure 3
Spectral response of the CCD detector

2.3 Expected beam dimensions

The LHC normalized emittance is $\varepsilon_n = 3.75$ μm [1] so that the emittance $\varepsilon = \varepsilon_n/\gamma$ is very small ($\gamma = \mathrm{E/E_0} = [1 - \beta^2]^{-1/2}$).

Some values of $\sigma = \sqrt{(\beta_{H,V}\varepsilon_n/\gamma)}$ or $\sigma[\mu m] = 59\sqrt{\beta[\mathrm{m}]/\mathrm{E[TeV]}}$ are given in Table 1, for $\beta = 100$ m. Thus very narrow profiles have to be resolved.

Table 1

Beam dimensions (r.m.s) for $\beta_{H,V} = 100$ m

E [TeV]	0.45	1	4	8
σ [μm]	884	593	295	210

3. ESTIMATION OF THE EMITTED POWER

Concerning the emitted power three possibilities are analysed, which are the emission:

- from a normal bending dipole,
- from a 'short' magnet,
- at the edge of a dipole.

It is important to remember that the SR is polarized in each of these three cases. One component (designated by the index '$\|$' or 'σ') is parallel and the other (designated by the index '$\perp$') is orthogonal to the particle-acceleration vector. This will be useful when considering the influence of natural diffraction.

In all three cases the radiated power in the parallel plane amounts to about 7/8 of the total radiated power.

Concerning the wavelength λ, taken into account in the computations, we have selected three ranges which are (λ in nm):

$$R_1 = [\lambda_2 = 150,\ \lambda_1 = 300], \quad R_2 = [400, 650], \quad R_3 = [350, 1100]\ .$$

This choice is not arbitrary and it will appear to be consistent:

- when taking into consideration the arguments developed in the section on diffraction,
- when considering the type of detector used, since each power spectrum will be weighted by d_2 for the ranges R_2 and R_3 and d_1 for R_1 (see par. 2.2).

3.1 Power emitted by a superconducting dipole

The expression for the emitted power P can be found in many publications [3] and is given by the following formula, for one particle:

$$\frac{\mathrm{d}P}{\mathrm{d}\omega} = \frac{P_0}{\omega_c} f\left(\frac{\omega}{\omega_c}\right) = \frac{P_0}{\omega_c} \frac{9\sqrt{3}}{8\pi} \left(\frac{\omega}{\omega_c}\right) \int_{\omega/\omega_c}^{\infty} \mathrm{K}_{5/3}\left(\frac{\omega}{\omega_c}\right) \mathrm{d}\left(\frac{\omega}{\omega_c}\right)\ ,$$

where

- $\omega_c = (3/2)\ (c\gamma^3/\rho) = 2\pi\nu_c$, ν_c being the critical frequency in s^{-1},
- ρ is the bending radius in m ($\rho = 2568$ m for LHC),
- $\mathrm{K}_{5/3}$ is the modified Bessel function of order 5/3,
- $\mathrm{P}_0 = (1/4\pi\varepsilon_0)\ (2/3)\ (ce^2\gamma^4/\rho^2)$ J.s^{-1}.

If we look at the power detected within a given frequency interval [ν_1, ν_2]

$$P[W] = 2\sqrt{3}\ \frac{e^2}{4\pi\varepsilon_0}\ \frac{\gamma}{\rho} \int_{\nu_1}^{\nu_2} \left(\frac{\nu}{\nu_c}\right) \left[\int_{\frac{\nu}{\nu_c}}^{\infty} \mathrm{K}_{5/3}(\eta)\ \mathrm{d}\eta\right]\ \mathrm{d}\nu$$

with

$$2\sqrt{3}\frac{\mathrm{e}^2}{4\pi\varepsilon_0} \simeq 8 \times 10^{-28}\ \mathrm{J.m}$$

Application to LHC

In Appendix A1 the power P_i emitted by one proton over the whole circumference and the power P_t emitted by 10^{14} protons over an arc of 1 mrad (since $1/\gamma \simeq 10^{-3}$, 1 mrad corresponds to a typical source length) are given for different energies such that:

$$P_\mathrm{t} = P_\mathrm{i}\ 10^{14} \times \frac{10^{-3}}{2\pi}\ .$$

Different ranges of wavelengths are considered ($\lambda = c/\nu$) such as:

a) range R_1 weighted by detector 1;
b) range R_2 weighted by detector 2;
c) range R_3 weighted by detector 2 .

If a minimum for a given detector is taken as a few 10^{-12} W, it can be seen that no profile can be observed when the proton energy is less than

0.8 TeV for case (c)	(visible to infrared range)
0.9 TeV for case (b)	(short end of visible range)
1.15 TeV for case (a)	(near ultraviolet range) .

This means that no profile can be observed when using the radiation emitted by superconducting dipoles for p energies which are lower than 1 TeV. At energies which are larger than 2 TeV the emitted light looks quite sufficient. One may refer to Appendix A2 for more details.

With this type of light source the problems of depth of field must be considered with care.

3.2 Short magnet

We have seen that when using the dipole radiation, even with a high intensity beam (10^{14} p), with the present commercial light detectors it looks impossible to obtain a transverse profile if the proton energy is less than about 1 TeV.

It is therefore worthwhile looking at the concept of a 'short magnet' of which the edge effect is a special case (see subsection 3.3). For this purpose we will use the computations of Ref. [4].

By 'short magnet' we consider that the radiation is emitted over a magnetic length 'L' such that

$$L \leq L_0 = \frac{m_0 c}{eB}$$

(for $E = 7.7$ TeV, $L_0 = 0.31$ m; $E = 450$ GeV, $L_0 = 5.35$ m). Since the synchrotron radiation is emitted within an angle $1/\gamma$, L_0 is the characteristic source length: $L_0 = \rho \cdot 1/\gamma$.

For a short dipole magnet which has a magnetic field of the form (Lorentz shape) (Fig. 4)

$$B(z) = \frac{B_0}{1 + (z/L)^2} ,$$

where z is the coordinate along the beam, the spectral energy distribution per particle is

$$\left(\frac{\mathrm{d}W}{\mathrm{d}\nu}\right)_{\mathrm{sm}} = \frac{\pi^3 C_1^2}{4c^2} B_0^2 L^2 \int_1^\infty (y^{-2} - 2y^{-3} + 2y^{-4})\, \mathrm{e}^{-xy}\, \mathrm{d}y ,$$

where C_1 is a constant;

$$C_1 = \left(\frac{e^2}{\pi m}\right) \left(\frac{1}{\varepsilon_0 c}\right)^{1/2} = 9.45 \times 10^{-11}\ \mathrm{m}^{3/2}\ \mathrm{s}^{-1/2} \text{ for protons}$$

$$x = \frac{4\nu}{\nu_1}, \qquad \nu_1 = \frac{2\gamma^2 c}{\pi L}.$$

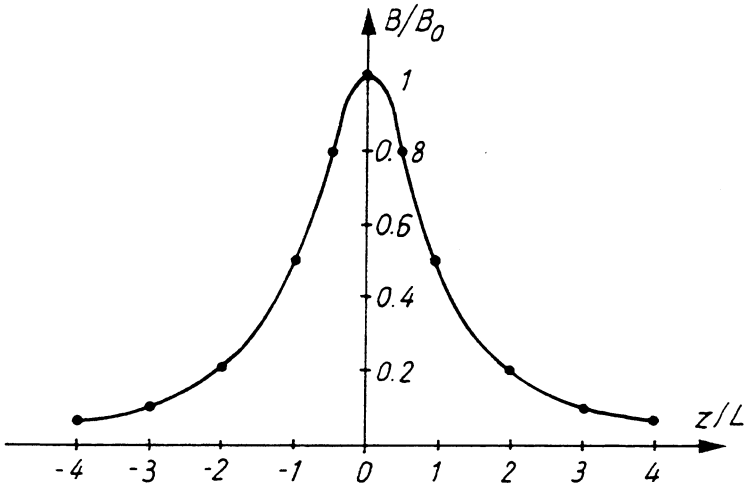

Figure 4

Shape of the 'short magnet' field

If we now consider the spectral power distribution collected in the spectrum range $[\nu_1, \nu_2]$ we thus get

$$P_{\mathrm{sm}} = \frac{\pi^3 C_1^2}{4c^2} B_0^2 L^2 N_{\mathrm{p}} f_{\mathrm{rev}} \int_{\nu_1}^{\nu_2} \left\{ \int_1^{\infty} \left(y^{-2} - 2y^{-3} + 2y^{-4} \right) \mathrm{e}^{-xy} \, \mathrm{d}y \right\} \mathrm{d}\nu \,,$$

where N_{p} = number of circulating protons, f_{rev} is the frequency of revolution,

$$P_{\mathrm{sm}} = 77 \times 10^{-37} B_0^2 \cdot L^2 \cdot N_{\mathrm{p}} \cdot f_{\mathrm{rev}} \int_{\nu_1}^{\nu_2} \left\{ \int_1^{\infty} \left(y^{-2} - 2y^{-3} + 2y^{-4} \right) \mathrm{e}^{-(4\nu/\nu_1)y} \, \mathrm{d}y \right\} \mathrm{d}\nu \,.$$

Application to LHC

Let $B_0 = 1$ T, $N_{\mathrm{p}} = 10^{14}$ p, $f_{\mathrm{rev}} = 11$ kHz. It must be noted that $B(z = 3L) = (1/10)\, B(z = 0)$. Appendix B gives the expected emitted power for $L = 0.15$ m and different spectrum ranges. The computations are made for energies ranging from 0.45 to about 1 TeV, and for higher energies where they are subject to caution since then L may become equal to L_0.

It can be seen that at full intensity ($N_{\mathrm{p}} = 4 \times 10^{14}$ p), when considering a large bandwidth detector and a very short magnet ($L = 0.15$ m), a profile could be observed. On the other hand, for energies larger than 1 TeV the radiation is sufficiently intense to allow reduction of the magnetic field B_0 and/or the spectrum range. Of course, this is a theoretical application and the exact computations must be made when knowing the magnetic field distribution, which could be similar to $B(\mathrm{z}) = B_0 \times \exp(-z^2)$, as computed in Ref. [5].

Since the light is emitted over a short distance the problems concerning the depth of field are greatly reduced.

3.3 Edge effect

The edge effect is relevant to the radiation emitted by the edge of a dipole where the magnetic field drops over a short distance. Good results have been obtained at the SPS at 450 GeV/c with 10^{13} p [6].

The theoretical analysis follows that used for a short magnet (Section 3.2 and Ref. [4]). If a magnetic field distribution (see Fig. 5)

$$B(z) = B_0 \left[\frac{1}{2} + \frac{1}{\pi} \arctan \frac{z}{L}\right] = \frac{B_0}{\pi L} \frac{1}{1+(z/L)^2} \times H(z)$$

is taken, where $H(z)$ is the Heaviside distribution, the following expression is obtained:

$$\left(\frac{\mathrm{d}W}{\mathrm{d}\nu}\right)_{ee} = \frac{\pi C_1^2}{c^2} B_0^2 L^2 \frac{1}{x^2} \int_1^\infty \left(y^{-2} - 2y^{-3} + 2y^{-4}\right) \mathrm{e}^{-xy}\, \mathrm{d}y \,,$$

and therefore for N_p protons

$$P_{ee} = \frac{\pi C_1^2}{c^2} B_0^2 L^2 \cdot N_p \cdot f_{\mathrm{rev}} \cdot \int_{\nu_1}^{\nu_2} \left[\int_1^\infty \left(y^{-2} - 2y^{-3} + 2y^{-4}\right) \mathrm{e}^{-xy}\, \mathrm{d}y\right] \frac{\mathrm{d}\nu}{x^2} \,.$$

Application to LHC

B_0 is of course in this case dependent on the p-beam energy ($B_0 = 10$ T for $E = 7.7$ TeV)

$$N_\mathrm{p} = 10^{14}\mathrm{p}, \quad f_{\mathrm{rev}} = 11\ kHz, \quad L = 2.5 \text{ cm} \,.$$

We use the preliminary conclusions of Ref. [7], where the computations show that the magnetic field drops to 10% of its nominal value over a distance of 15 cm $= 6L$.

Appendix C gives the results of computations for two different wavelength ranges.

It can be seen that for detectors operating in the visible range a profile could be observed from injection energy with the LHC working at full intensity. However no suitable layout has been found for the extraction of the light.

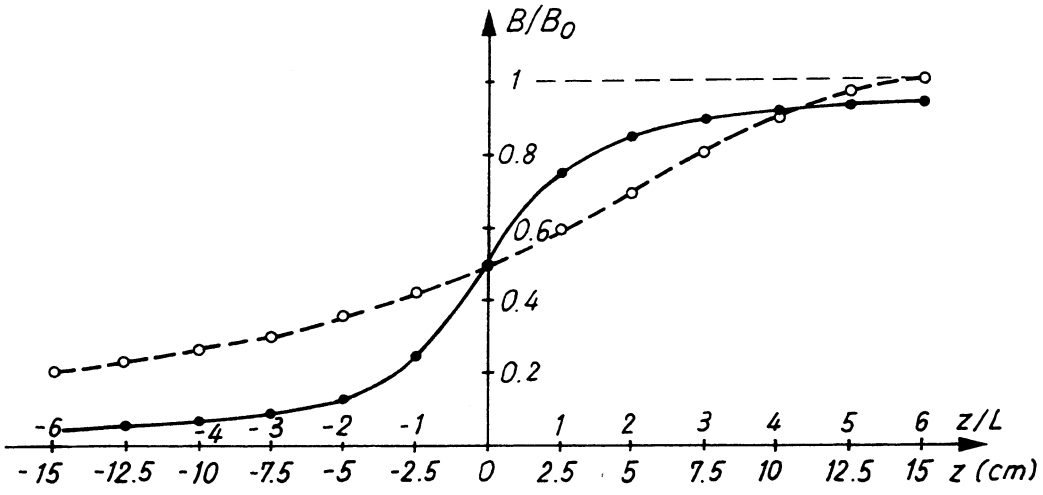

Figure 5

Shape of the magnetic field at the edge of a dipole (continuous line) and the scaled Lorentz edge shape (broken line) given in subsection 3.2

4. DIFFRACTION

Owing to the fact that the SR appears in the laboratory frame within a small solid angle (of the order of $1/\gamma$) rather than isotropically, the p-beam image will suffer from diffraction. This 'natural diffraction' will introduce errors in the measurement of the beam profile. The relative disturbance will depend on the actual proton-beam dimensions, given by the r.m.s. width (see Section 2.2) and the observed frequency range $[\nu_1, \nu_2]$.

Fraunhofer diffraction is, in this case, relevant since, as already mentioned, SR is emitted within a small angle. The procedure given in Ref. [8] should be followed.

Computations have been made elsewhere [9]. We will only look at the 'short magnet' case (the 'edge effect' gives similar results).

As an introduction it is worth while recalling the diffraction from classical appertures on a *monochromatic* source object [8].

4.1 Diffraction from classical apertures

Let a point source emit a monochromatic light (wavelength: λ) uniformly distributed in space. If the light waves are intercepted by a slit of width D, the diffraction radius r_d at a distance R (see Fig. 6) is given by

$$r_d = \frac{\lambda R}{D}$$

In the case of a uniform radiation passing through a circular aperture of diameter ϕ:

$$r_d = 1.22 \cdot \frac{\lambda R}{\phi} .$$

Finally, if instead of a physical aperture we have a light angular distribution of r.m.s. opening σ_α we come to about

$$\sqrt{< r_d^2 >} = \sigma_d \simeq \frac{1}{2\pi\sqrt{2}} \frac{\lambda R}{\sigma_\alpha} .$$

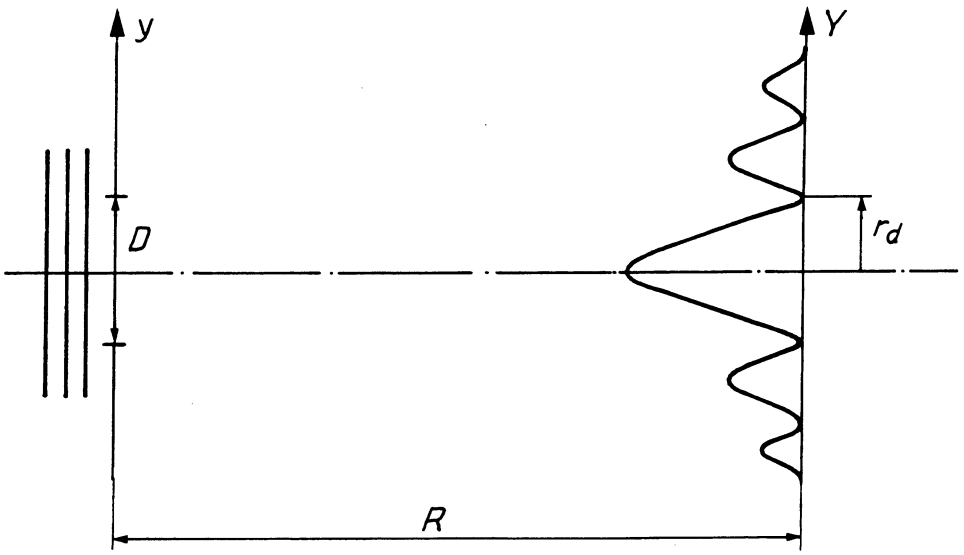

Figure 6

Description of the symbols used for the diffraction from a slit

For SR, since the wave amplitudes have various distributions the 'diffraction r.m.s spot size σ_d' must be computed specifically.

Let us recall from Section 2.3 that the p-beam r.m.s dimension σ is

$$\sigma = \sqrt{(\beta_{H,V}\varepsilon_n/\gamma)}$$

The image will therefore have a r.m.s. width

$$r_i = \sqrt{\sigma^2 + \sigma_d^2} > \sigma \ .$$

The diffraction effect induces errors on the measurement of the beam width.

4.2 Diffraction from a 'short magnet'

The SR is emitted within a small solid angle.

Following the procedure described in Ref. [4] and using the symbols of Fig. 7, the diffraction pattern is the modulus square of the amplitude of diffraction F given by

$$F(\psi',\varphi') = \int_{\psi=0}^{\psi=\infty} \int_{\varphi=0}^{2\pi} f(\psi,\varphi,\psi',\varphi') e^{-j\psi\psi'\cos(\varphi-\varphi')}\ \psi d\psi d\varphi \ ,$$

where

- $\psi = \gamma\theta = \dfrac{\gamma r}{p}, \quad \psi' = \dfrac{kr'}{\gamma}\dfrac{p}{p'} = \dfrac{2\pi}{\lambda}\dfrac{r'}{\gamma}\dfrac{p}{p'}, \quad \gamma = (1-\beta^2)^{-1/2}$,

- f can be split into two polarized components,

$$f_\perp = C\,\frac{\psi^2 \sin 2\varphi}{(1+\psi^2)^2}\,\hat{B}\left(\nu\,\frac{1+\gamma^2\theta^2}{2c\gamma^2}\right) \quad \text{orthogonal part}$$

$$f_{||} = C\,\frac{(1-\psi^2\cos 2\varphi)}{(1+\psi^2)^2}\,\hat{B}\left(\nu\,\frac{1+\gamma^2\theta^2}{2c\gamma^2}\right) \quad \text{parallel part} \ .$$

ν is the observed frequency, $\hat{B}$ the Fourier transform of the 'short magnet' magnetic field, and C a constant.

The diffraction pattern is given by $|F(\psi',\varphi')|^2$. We consider again the analytical example:

$$B(z) = \frac{B_0}{1+(z/L)^2} \ .$$

Then using the results of Ref. [6] and avoiding the constant terms, for a given frequency (or wavelength λ) we obtain

$$|F_\perp(\psi',\varphi')|^2 = \left|\sin(2\varphi') \int_0^\infty \frac{\psi^3 J_2(\psi\psi')}{[1+\psi^2]^2}\, e^{-x[1+\psi^2]}\, d\psi\right|^2$$

$$|F_{||}(\psi',\varphi')|^2 = \left|\int_0^\infty (J_0(\psi\psi') + \psi^2\cos(2\varphi')\, J_2(\psi\psi'))\, \frac{\psi^2}{[1+\psi^2]^2}\, e^{-x[1+\psi^2]}\, d\psi\right|^2 ,$$

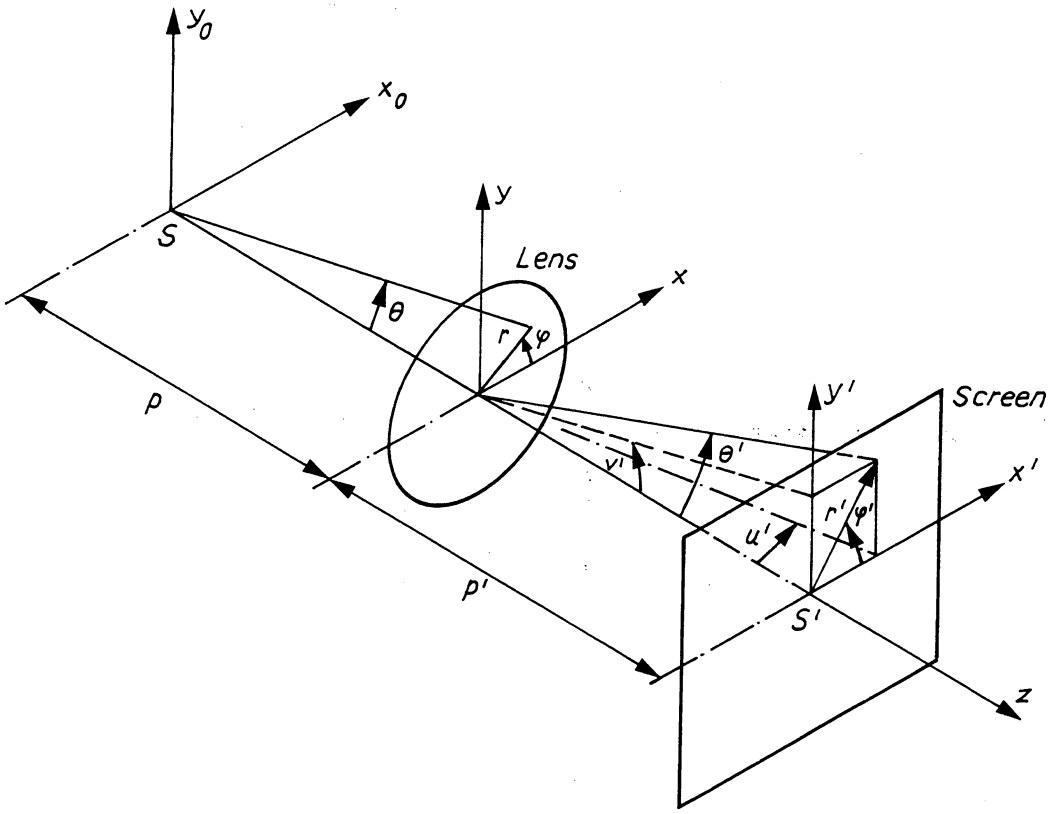

Figure 7

Symbols used for the diffraction computation

where J_0 and J_2 are the normal Bessel functions.

Computations can be made for a given φ'. However, ψ' and x are frequency dependent:

$$\psi' = \frac{2\pi}{\lambda}\, \mathrm{r}'\, \frac{\mathrm{p}}{\mathrm{p}'} = \frac{2\pi\nu}{c} \cdot \frac{\mathrm{p}}{\mathrm{p}'}\, \mathrm{r}', \qquad x = \frac{4\nu}{\nu_1},$$

where p/p', the magnification ratio, can be set at 1 without any loss of generality.

If we integrate over the detector bandwidth (which has a response considered here to be uniform):

$$|F_*(r', \varphi')|^2 = \left| \int_{\nu_1}^{\nu_2} F_*(x', \varphi', \nu)\, \mathrm{d}\nu \right|^2,$$

where * = (|| or σ) or $\perp$ planes.

The shapes of some diffraction patterns are given by Fig. 8 (for the parallel polarization and $\varphi' = 0$) and Fig. 9 (for the parallel polarization and $\varphi' = \pi/2$). The values of σ_d are given for the values of r' such as $|F_\sigma|^2_{r'=r_\mathrm{d}} = 0.6$, which corresponds to the r.m.s. value of a Gaussian distribution.

Table 2 gives the computed r.m.s. values of the diffraction pattern, in micrometres:

- for the parallel polarization component,
- for two different angles $\varphi' = 0$ (Table 2a) and $\varphi' = \pi/2$ (Table 2b),
- for different wavelength ranges (the detector spectral response has been considered constant within each spectrum range).

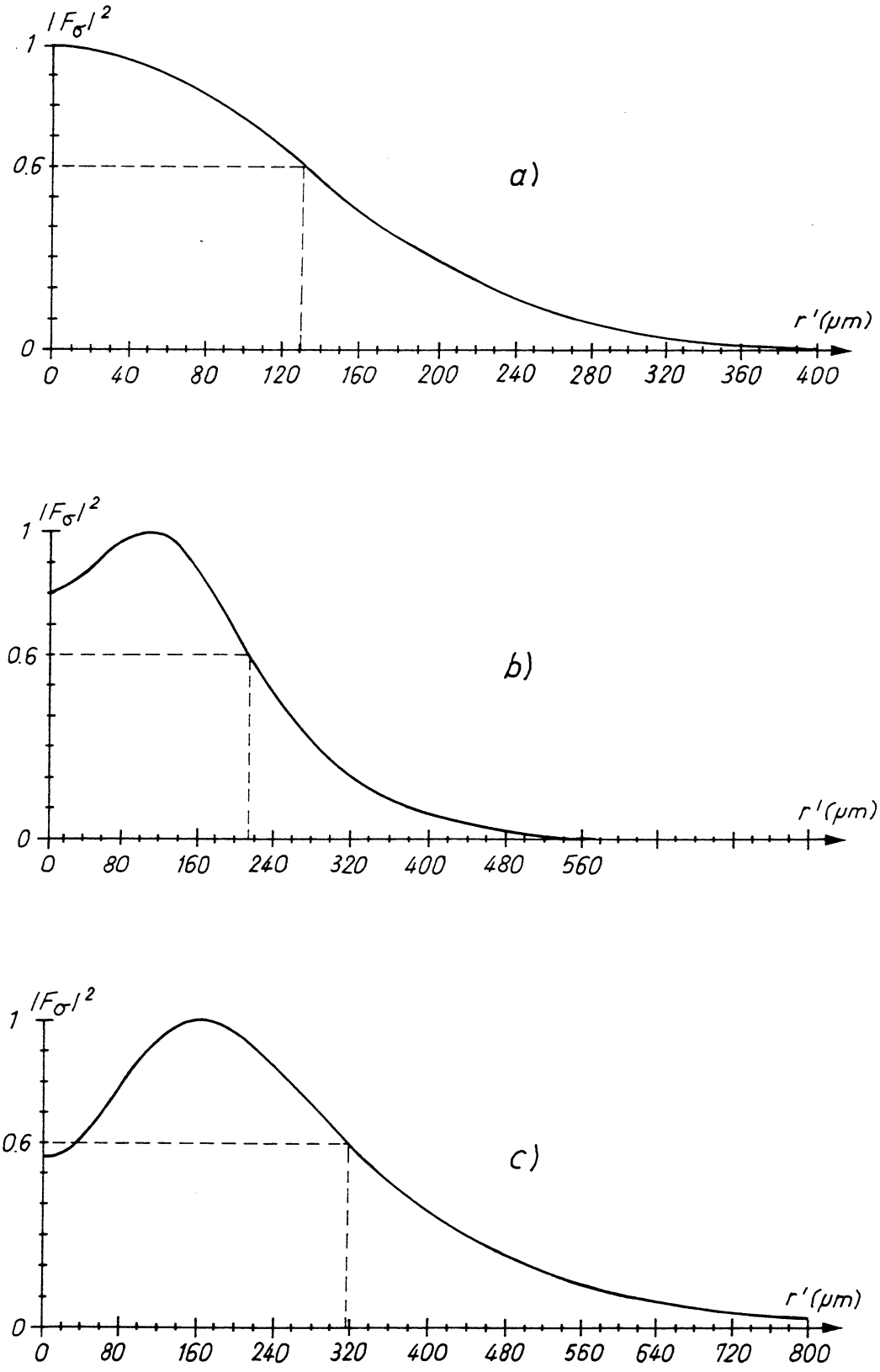

Figure 8

Diffraction pattern $|F_\sigma|^2$ in the direction $\varphi' = 0$

a) E = 0.45 TeV, $\lambda_1 = 800$ nm, $\lambda_2 = 600$ nm
b) E = 4 TeV, $\lambda_1 = 250$ nm, $\lambda_2 = 150$ nm
c) E = 8 TeV, $\lambda_1 = 250$ nm, $\lambda_2 = 150$ nm

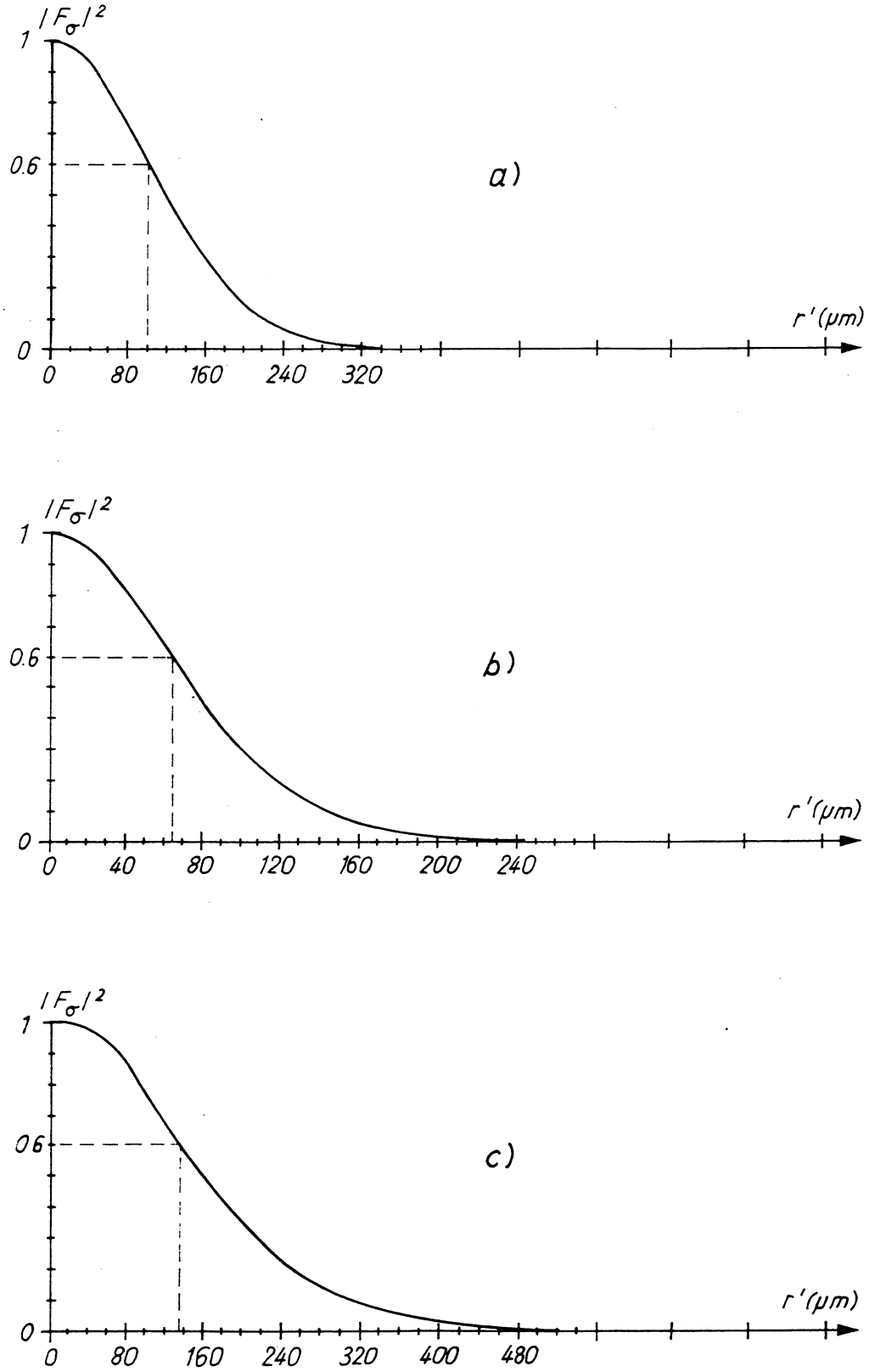

Figure 9

Diffraction pattern $|F_\sigma|^2$ in the direction $\varphi' = \pi/2$

a) E = 0.45 TeV, $\lambda_1 = 800$ nm, $\lambda_2 = 600$ nm
b) E = 4 TeV, $\lambda_1 = 250$ nm, $\lambda_2 = 150$ nm
c) E = 8 TeV, $\lambda_1 = 250$ nm, $\lambda_2 = 150$ nm

Table 2a

Diffraction broadening $\sigma_d[\mu m]$ in the horizontal direction ($\varphi' = 0$)

	E [TeV]			
Range [nm]	0.45	1	4	8
150–250	60	90	215	315
450–550	102	170	480	680
600–800	130	230	600	920

Table 2b

Diffraction broadening $\sigma_d[\mu m]$ in the vertical direction ($\varphi' = \pi/2$)

	E [TeV]			
Range [nm]	0.45	1	4	8
150–250	55	56	65	130
450–550	90	92	110	140
600–800	100	115	130	140

For high energies a flattened distribution (vertical diffraction lower than the horizontal diffraction) is observed.

The values of Table 2 should be compared with those of Table 1.

We could foresee 'substracting' σ_d from the measured profile. This must be considered with care since the diffraction pattern is dependent on φ'.

5. POSSIBLE LAYOUTS

According to what has been estimated concerning the detected powers and spectra, it appears clear that at least two important points remain to be solved, which concern the image detector itself and the installation of the mirror that extracts the radiated light from the vacuum tube.

We have also seen that the use of a short magnet looks promising for the coverage of the full energy range.

By *'Telescope'* we mean the Mirror + Optics + Detector as a whole. It will be described in Section 6.

The mirror must, of course, see the light emitted by the source and not be hit by the p beam. As a consequence, a bending magnet must be located between the source and the mirror.

In the following we only consider the light generated from the high field of a superconducting dipole or that from a short magnet.

5.1 Layout of the light extraction from a superconducting dipole

The installation of the mirror should be avoided in the cryogenic environment, where prohibitive difficulties may arise.

a) Use of the edge field.

According to the beam-pipe dimensions, the light emitted at one edge of a normal cell dipole does not escape at the other end. Therefore, the only possibility would be to use the edge of the last arc dipole.

This is not possible, since the light is emitted alongside the beam.

b) Light source located inside a superconducting dipole.

Two possibilities exist: near Q10 or near Q6, see Fig. 10. Q10 must be discarded because of the large Dx value. Amongst the five insertion optics the dumping one is by far the best: beta values are convenient and do not change during ramping. In the middle of the last B3:

$$\beta_{\mathrm{H}} = 38 \text{ m}, \ \beta_{\mathrm{V}} = 126 \text{ m} .$$

Using enlarged quadrupoles for Q6 ($\phi = 75$ mm $- 7$ mm), the extraction mirror can be located at 24 m from the source. A mirror with $\Delta x = 30$ mm has a r.m.s. acceptance $\sigma_\theta \approx 300$ μrad corresponding to a field depth $\sigma_z = \sigma_\theta \, \rho = 0.8$ m, which is acceptable. The layout is shown in Fig. 11.

Table 3 summarizes the diffraction properties.

Table 3

Data for the light extraction from a source in a superconducting dipole

E [TeV]	λ [nm]	σ_{H} [μm]	σ_{dh} [μm]	σ_{V} [μm]	σ_Ψ [μrad]	σ_{dv} [μm]
1	500	366	188	666	235	240
2	250	259	94	471	186	152
4	180	183	68	333	167	122
8	180	129	68	235	167	122

$\sigma_{\mathrm{H,V}} = 59 \sqrt{\beta_{\mathrm{H,V}}/E}$ r.m.s beam dimension

$\sigma_{\mathrm{dh}} = 0.113 \, \lambda/\sigma_\theta$ r.m.s horizontal diffraction

$\sigma_\Psi = 0.756 \, (\lambda/2\pi\rho)^{1/3}$ r.m.s angular distribution

$\sigma_{\mathrm{dv}} = 0.113\lambda/\sigma_\Psi$ r.m.s vertical diffraction

Below 1 TeV there is not enough energy for the detector (see Appendix A), from 1 TeV up to 8 TeV the diffraction broadening is $\leq 13\%$, which is quite acceptable. The value D$x = -0.07$ m can be neglected.

5.2 Layout of light extraction from the D2 edge and from a short magnet

The D2 magnets are the only ones which offer a favourable geometry for a synchrotron light extraction, see Fig. 12.

An edge is well localized along the beam line and produces a nearly punctual source at injection energy (see Appendix C). But at top energy the uniform dipole field dominates and the source extends over the whole field depth of the optical system, collecting a lot of diffused light.

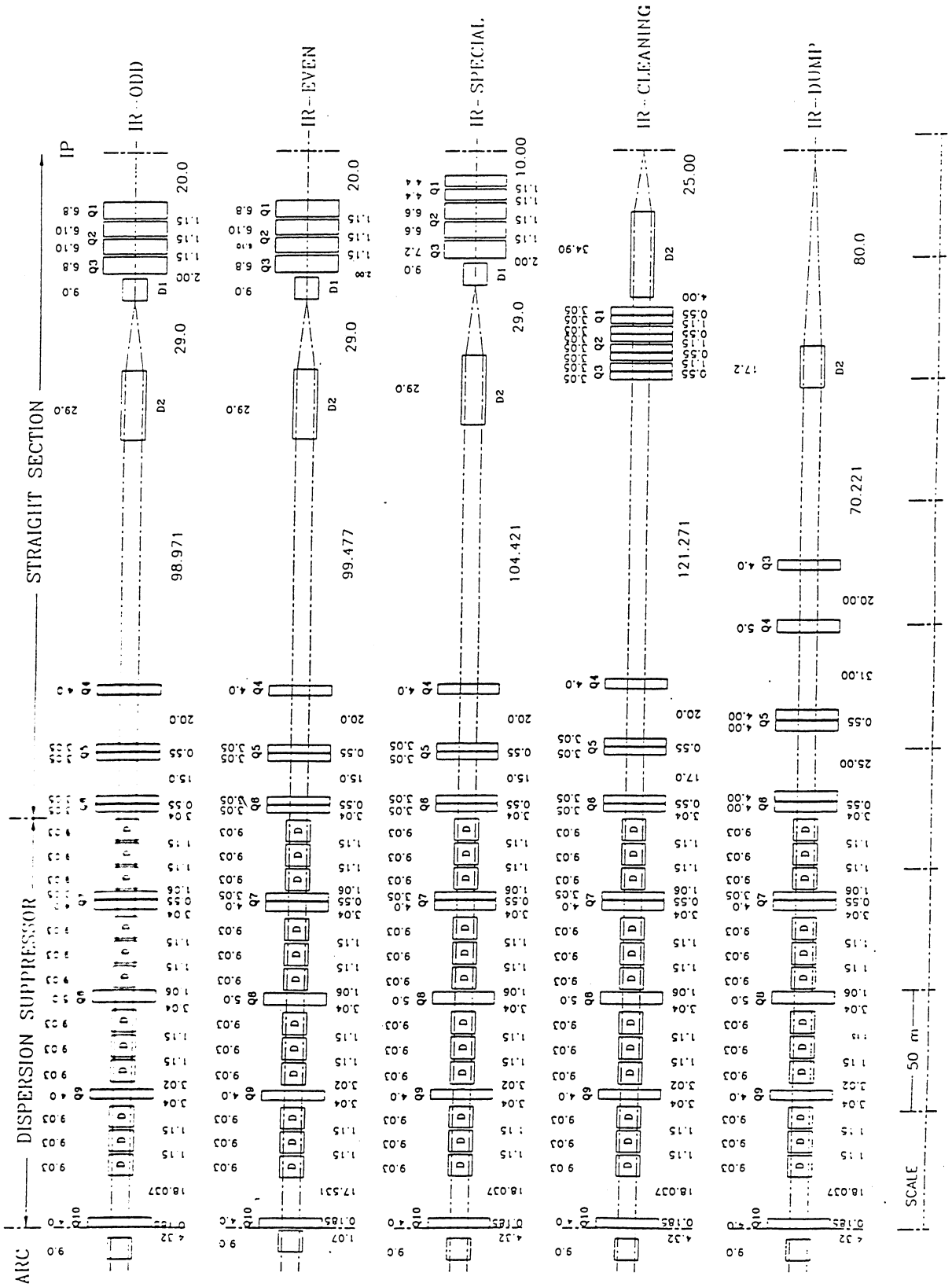

Figure 10

Experimental and machine insertions

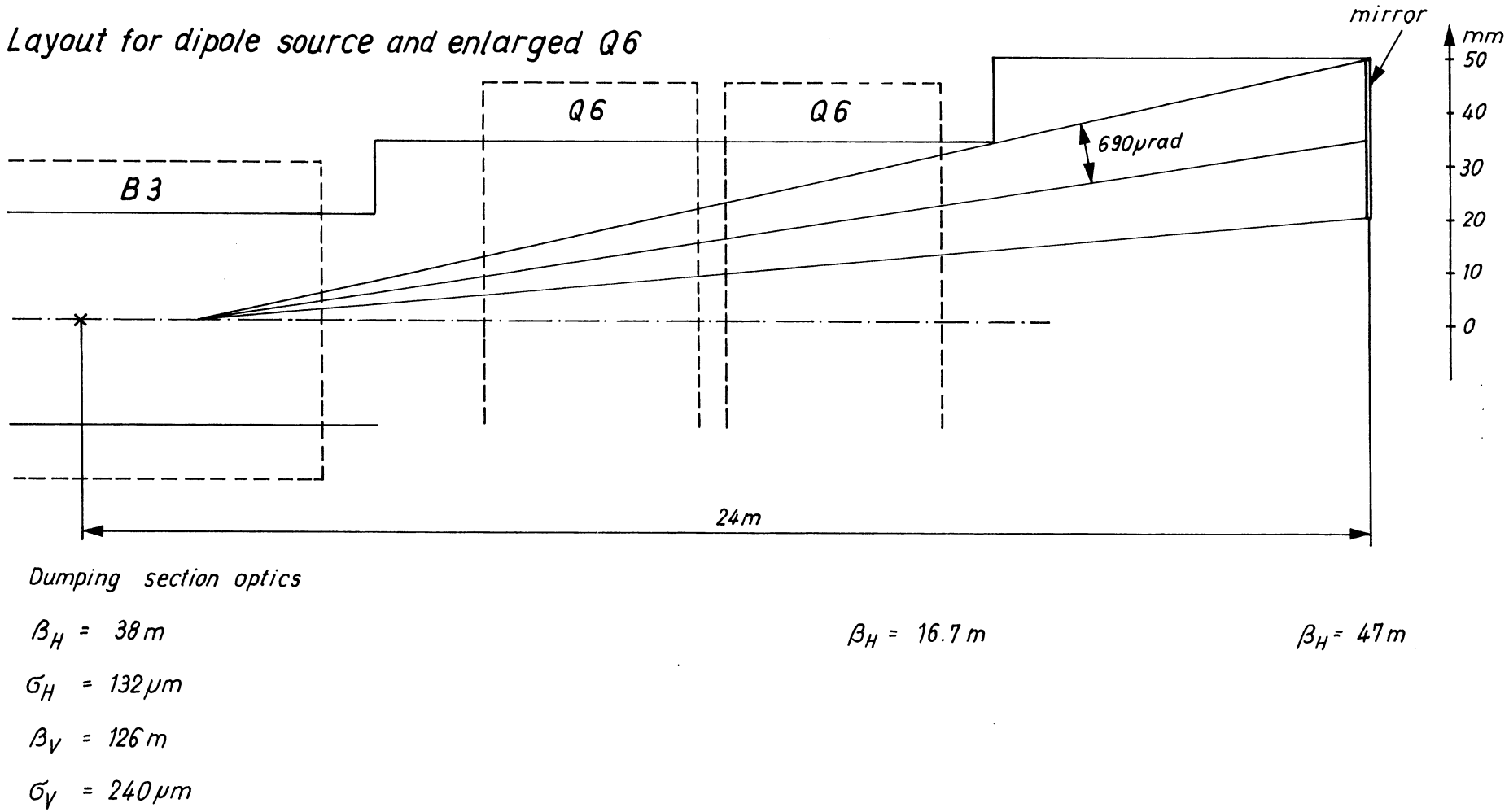

Figure 11

Layout of the light extraction from a supraconducting dipole

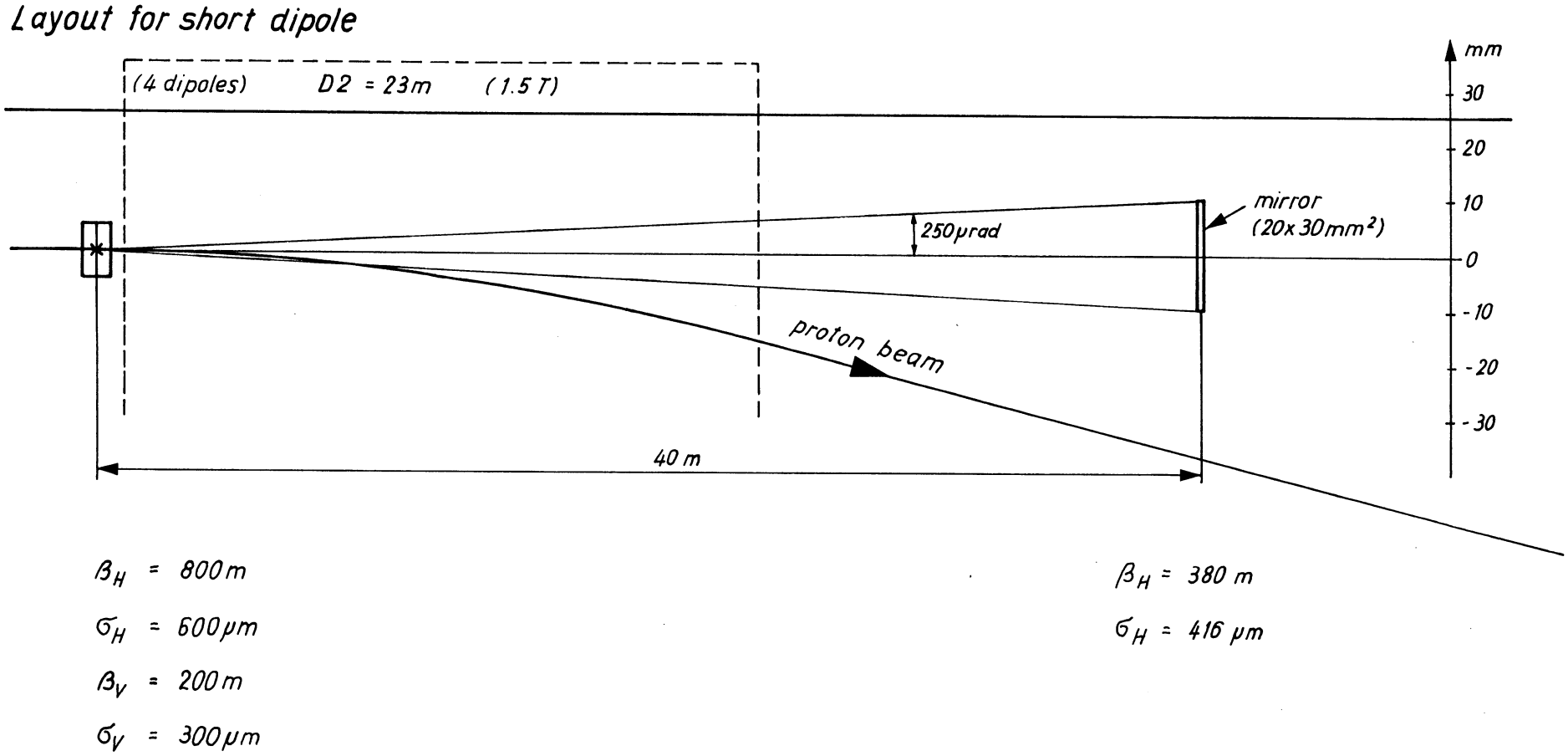

Figure 12

Layout of the light extraction from a short magnet

If the D2 magnet is run at a field $B_0 \leq 1.5$ T no significant light is produced in the LHC energy range. In these circumstances the edge field is too small and a short magnet is required in front at D2. Even better, three short magnets of opposite signs would be neutral for the orbit and could therefore be powered independently of beam energy.

The layout shown in Fig. 12 is similar to the beam dump insertion with longer D2 magnets, but would require *special optics* in order to provide adequate beam sizes at the source ($\beta_H = 800$ m and $\beta_V = 200$ m) and no dispersion.

With a photon-beam acceptance of 20 mm × 30 mm at the extraction mirror, the diffraction properties given in Table 4 can be reached.

Table 4

Data for the light extraction from an edge or a short magnet

E [TeV]	λ [nm]	σ_H [μm]	σ_θ [μrad]	σ_{dH} [μm]	σ_V [μm]	σ_Ψ [μrad]	σ_{dV} [μm]
0.45	500	2500	125	450	1250	188	300
1	500	1678	125	450	839	188	300
4	200	839	105	215	419	188	120
8	200	593	72	315	297	174	130

From inspection of Table 4 it is seen that the diffraction r.m.s spot size σ_d is always smaller than half the r.m.s beam size and will therefore affect the measured beam size by less than 12%.

6. THE TELESCOPE

The design of the telescope is based on the experience gained with the LEP synchroton light monitors [2]. We are assuming the use of the light originating from the dedicated short magnet. (see Fig. 12)

The general layout of the telescope is given in Fig. 13. Its components are mounted on a standard optical bench of 3.2 m length. The telescope only uses mirrors so as to be perfectly achromatic. A second detector, comprised only of a CCD chip, can be driven in place of the composite detector represented.

The vertically polarized component of the SR is highly attenuated through large-angle metallic reflections in the first two mirrors and can be neglected afterwards.

The origin of the light can be restricted by a slit located in the focal plane of the focusing mirror. The wavelength filters will define the spectral window for best sensitivity and minimum diffraction in normal operation. At least two extra wavelength filters will be installed in order to measure precisely, and hence correct later, the contribution of the diffraction to the measured profiles. A total of seven filters distributed over the spectral range of the detectors is foreseen.

Density filters will adjust the available SR power to the dynamic range of the detectors for the best signal-to-noise ratio. Seven filters are proposed, with transmissions between 100% and 0.1% in 5 dB steps.

The optical magnification of the telescope has been assumed to be $G = 0.4$, which gives an acceptance of ±8 mm in the vertical plane and ±11 mm in the horizontal plane with the detector under consideration. A different magnification can be implemented if necessary.

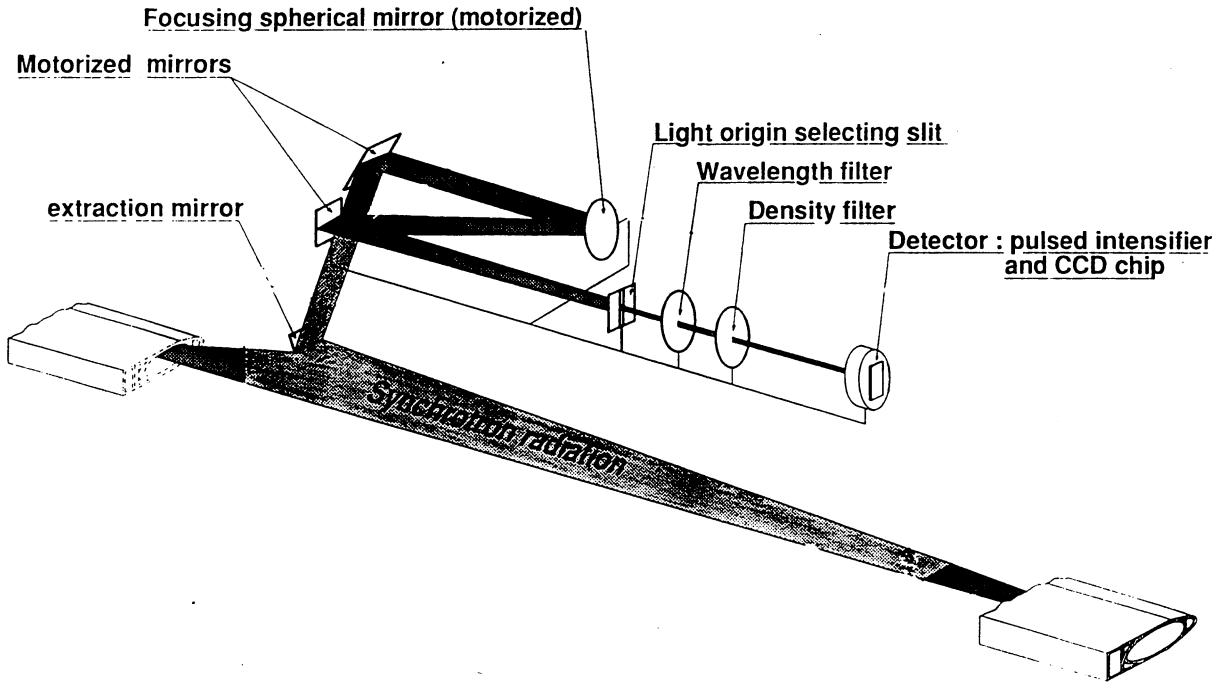

Figure 13

Simplified schematic layout of the synchrotron radiation telescope (taken from LEP)

The detectors considered for the various estimations use the same CCD chip as the one used in the LEP monitor, i.e. the TH 7863 from Thomson. It is probable that better detectors will be available when this monitor is built, with higher sensitivity, better spatial resolution and less noise for High Definition TV. An intensifier, which can be pulsed, will be used to increase the sensitivity of the monitor (gain of up to 10^4) and to shift the observable spectral window down to the UV domain in order to decrease the contribution of the diffraction to the measured profiles. However, in the present state of the technology, the overall gain on the spatial performance is not improved because of the additional broadening introduced by the intensifier.

The various contributions to the broadening of the measured profiles have been estimated in a Gaussian approximation and have been added quadratically to the beam profile.

It will be possible to measure these quantities precisely with beam in the LHC.

With these assumptions, it is possible to estimate the performance of the monitor. This performance is summarized in Appendix D for the short magnet case. A circulating beam of 10^{14} particles and an intensifier with a maximum gain of 10^4 have been assumed. The gain of the intensifier, the density filters, and the integration time of the CCD have been chosen within reasonable limits for best performance.

From the table in Appendix D it can be seen that for circulating beams of 10^{14} particles the monitor can measure profiles from 450 GeV to 8 TeV, under the assumption that the parameters are changed and adapted to the situation during the ramp. Beams of 10^{12} p can be measured with an acceptable signal-to-noise ratio at 450 GeV with the

large bandwidth intensifier.

The data can be acquired either pixel by pixel for best spatial resolution or by a frame grabber for fast video mode acquisition. The digitization is done over 8 to 12 bits. Improvements are also expected in this field. The data are then processed to extract the emittances and fed into the control system. It is vital to foresee a live TV link to the control room and to superimpose on the TV picture the digital information extracted. The detailed digital and graphical information will be available on work stations for analysis and archiving. A logging facility has also to be foreseen for cross-correlations and further machine studies.

7. CONCLUSIONS

It has been shown that an accurate measurement of LHC transverse profiles using synchrotron radiation is difficult for two main reasons:

- Firstly, at low energies (i.e. 0.45 to 1.5 TeV) the power radiated in a superconducting dipole is insufficient and a dedicated short magnet would have to be implemented as a dedicated source.
- Secondly, at high energies (i.e. from 4 to 8 TeV) the light diffraction, even at short wavelength, is limiting the accuracy of beam size measurements.

A telescope looking through Q6 at the light emitted in the last superconducting dipole is very effective for energies above 1.5 TeV, but cannot be used at injection.

In order to cover the full energy range, a dedicated short magnet needs to be installed in a stright section provided with special fixed optics (β_H = 800 m, β_V = 200 m, Dx = 0 at the short magnet position). The light produced by the beam in this short magnet is observed with a measuring telescope through a weak D2 magnet necessary to deflect the protons away from the extraction mirror. A problem might arise at top energy due to the SR produced in the higher field of the D2 magnet, which could create a detrimental background.

Therefore building both systems might be required, in view of their complementarity.

REFERENCES and FOOTNOTES

[1] The LHC Study Team, Design study of the Large Hadron Collider (LHC) a multiparticle collider in the LEP tunnel, CERN/AC/DI/FA/90–06 (1990).

[2] C. Bovet et al., The LEP synchrotron light monitors, Proceedings of the PAC Conference, San Francisco, 1991.

[3] a) J.D. Jackson, Classical electrodynamics (J. Wiley, NY, 1976), Chapter on 'Radiation by moving charges'.
b) A. Hofmann, Characteristics of synchrotron radiation, CERN Accelerator School, Chester, 1989, CERN 90–03 (1990).

[4] R. Coïsson, Angular-spectral distribution and polarisation from a 'short magnet', Phys. Rev. **A20** (1979) 524.

[5] H.H. Umstätter, Magnet profile for Gaussian field distribution, PS/HI/Note 91–9, PS/BD/Note 91–3.

[6] R. Bossart, J. Bosser, L. Burnod, R. Coïsson, E.D'Amico, A. Hofmann and J. Mann, Observation of visible synchrotron radiation emitted by a high-energy proton beam at the edge of a magnetic field, Nucl. Instrum. Methods **164** (1979) 375–380.

[7] D. ter Avest, C. Daum and H.H.J. ten Kate, Magnetic fields and Lorentz forces in an LHC dipole magnet; 3-D analysis using the FEM program TOSCA, LHC Note 111, 1989.

[8] a) M. Born and E. Wolf, Principles of optics (Pergamon, NY, 1975), pp. 390–416.
b) M. Françon, Diffraction (Gauthier-Villars, Paris, 1964).

[9] A Hofmann and F. Meot, Optical resolution of beam-cross-section measurements by means of synchrotron radiation, CERN/ISR–TH/82–04 (1982).

Appendix A1

Emitted power of a LHC dipole

Proton energy (eV)	a) $\lambda_2 = 150$ nm, $\lambda_2 = 300$ nm, Detector 1		b) $\lambda_2 = 400$ nm, $\lambda_2 = 650$ nm Detector 2		c) $\lambda_2 = 350$ nm, $\lambda_1 = 1100$ nm Detector 2	
	Power emitted by 1 proton (W)	Power emitted by 10^{14} p over an arc of 1 mrad (W)	Power emitted by 1 proton (W)	Power emitted by 10^{14} p over an arc of 1 mrad (W)	Power emitted by 1 proton (W)	Power emitted by 10^{14} p over an arc of 1 mrad (W)
1.00×10^{12}	7.18×10^{-27}	1.14×10^{-16}	5.46×10^{-20}	8.70×10^{-10}	5.80×10^{-18}	9.23×10^{-8}
2.00×10^{12}	1.06×10^{-14}	1.68×10^{-4}	3.08×10^{-14}	4.90×10^{-4}	7.85×10^{-14}	1.25×10^{-3}
3.00×10^{12}	2.98×10^{-13}	4.74×10^{-3}	1.35×10^{-13}	2.15×10^{-3}	2.73×10^{-13}	4.34×10^{-3}
4.00×10^{12}	7.25×10^{-13}	1.15×10^{-2}	2.02×10^{-13}	3.21×10^{-3}	3.87×10^{-13}	6.16×10^{-3}
5.00×10^{12}	1.02×10^{-12}	1.63×10^{-2}	2.37×10^{-13}	3.77×10^{-3}	4.47×10^{-13}	7.11×10^{-3}
6.00×10^{12}	1.21×10^{-12}	1.93×10^{-2}	2.57×10^{-13}	4.09×10^{-3}	4.81×10^{-13}	7.65×10^{-3}
7.00×10^{12}	1.33×10^{-12}	2.12×10^{-2}	2.69×10^{-13}	4.28×10^{-3}	5.01×10^{-13}	7.98×10^{-3}
8.00×10^{12}	1.41×10^{-12}	2.24×10^{-2}	2.77×10^{-13}	4.41×10^{-3}	5.15×10^{-13}	8.19×10^{-3}
7.50×10^{11}			2.06×10^{-28}	3.28×10^{-18}	2.08×10^{-23}	3.30×10^{-13}
8.00×10^{11}			7.19×10^{-26}	1.14×10^{-15}	8.42×10^{-22}	1.34×10^{-11}
8.50×10^{11}			7.01×10^{-24}	1.12×10^{-13}	1.58×10^{-20}	2.51×10^{-10}
9.00×10^{11}			2.67×10^{-22}	4.25×10^{-12}	1.66×10^{-19}	2.65×10^{-9}
9.50×10^{11}			5.01×10^{-21}	7.97×10^{-11}	1.14×10^{-18}	1.82×10^{-8}
1.00×10^{12}	7.18×10^{-27}	1.14×10^{-16}	5.46×10^{-20}	8.70×10^{-10}	5.80×10^{-18}	9.23×10^{-8}
1.05×10^{12}	4.66×10^{-25}	7.42×10^{-15}	3.92×10^{-19}	6.23×10^{-9}	2.22×10^{-17}	3.54×10^{-7}
1.10×10^{12}	1.50×10^{-23}	2.38×10^{-13}	2.02×10^{-18}	3.21×10^{-8}	6.85×10^{-17}	1.09×10^{-6}
1.15×10^{12}	2.75×10^{-22}	4.37×10^{-12}	8.38×10^{-18}	1.33×10^{-7}	1.78×10^{-16}	2.84×10^{-6}
1.20×10^{12}	3.22×10^{-21}	5.13×10^{-11}	2.74×10^{-17}	4.36×10^{-7}	4.05×10^{-16}	6.45×10^{-6}
1.25×10^{12}	2.63×10^{-20}	4.19×10^{-10}	7.47×10^{-17}	1.19×10^{-6}	8.24×10^{-16}	1.31×10^{-5}
1.30×10^{12}	1.60×10^{-19}	2.54×10^{-9}	1.76×10^{-16}	2.81×10^{-6}	1.53×10^{-15}	2.43×10^{-5}

Appendix A2

One is looking at the proton energy E which results in a detected power of 10^{-12} W emitted, by superconducting dipoles, within a wavelength range [$\lambda_2 = 0.75\ \lambda_0$, $\lambda_1 = 1.25\ \lambda_0$].

For that purpose the formula of 3.1, giving the power detected within the frequency interval [$\nu_1 = c/\lambda_1$, $\nu_2 = c/\lambda_2$] is used. The corresponding curve is plotted in figure A2.

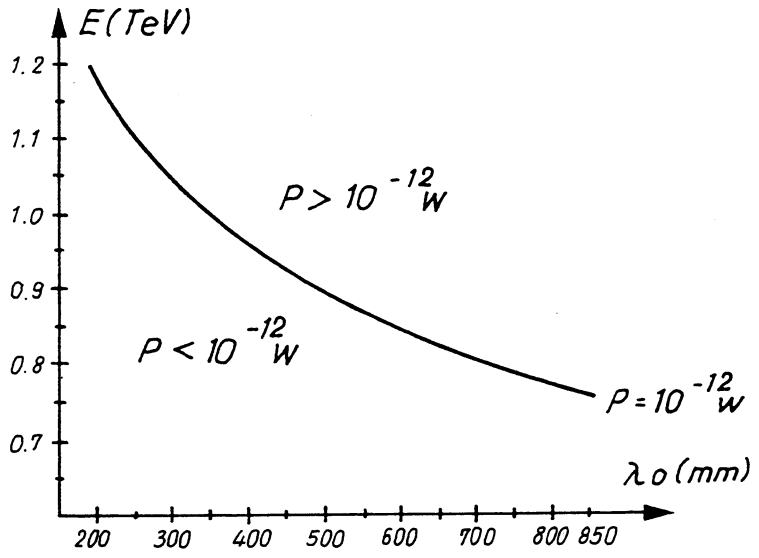

Figure A2
Energy E as a function of λ_0 for a detected power of 10^{-12} W

Appendix B

Power emitted by a 'short magnet' ($L = 0.15$ m)

a) $\lambda_2 = 150$ nm $\lambda_1 = 300$ nm detector 1		b) $\lambda_2 = 450$ nm $\lambda_1 = 650$ nm detector 2		c) $\lambda_2 = 350$ nm $\lambda_1 = 1100$ nm detector 2	
Proton energy (eV)	Total emitted power for 10^{14} p (W)	Proton energy (eV)	Total emitted power for 10^{14} p (W)	Proton energy (eV)	Total emitted power for 10^{14} p (W)
1.00×10^{12}	4.95×10^{-8}	1.00×10^{12}	1.42×10^{-7}	1.00×10^{12}	4.19×10^{-7}
2.00×10^{12}	1.44×10^{-6}	2.00×10^{12}	7.48×10^{-7}	2.00×10^{12}	1.84×10^{-6}
3.00×10^{12}	3.28×10^{-6}	3.00×10^{12}	1.23×10^{-6}	3.00×10^{12}	2.99×10^{-6}
4.00×10^{12}	4.81×10^{-6}	4.00×10^{12}	1.70×10^{-6}	4.00×10^{12}	4.20×10^{-6}
5.00×10^{12}	6.19×10^{-6}	5.00×10^{12}	2.27×10^{-6}	5.00×10^{12}	5.68×10^{-6}
6.00×10^{12}	7.62×10^{-6}	6.00×10^{12}	2.96×10^{-6}	6.00×10^{12}	7.48×10^{-6}
7.00×10^{12}	9.21×10^{-6}	7.00×10^{12}	3.77×10^{-6}	7.00×10^{12}	9.62×10^{-6}
8.00×10^{12}	1.10×10^{-5}	8.00×10^{12}	4.72×10^{-6}	8.00×10^{12}	1.21×10^{-5}
4.50×10^{11}	7.25×10^{-14}	4.50×10^{11}	1.92×10^{-10}	4.50×10^{11}	2.18×10^{-9}
5.00×10^{12}	1.40×10^{-12}	5.00×10^{11}	8.35×10^{-10}	5.00×10^{11}	6.66×10^{-9}
5.50×10^{11}	1.33×10^{-11}	5.50×10^{11}	2.55×10^{-9}	5.50×10^{11}	1.58×10^{-8}
6.00×10^{11}	7.72×10^{-11}	6.00×10^{11}	6.09×10^{-9}	6.00×10^{11}	3.13×10^{-8}
6.50×10^{11}	3.15×10^{-10}	6.50×10^{11}	1.22×10^{-8}	6.50×10^{11}	5.44×10^{-8}
7.00×10^{11}	9.89×10^{-10}	7.00×10^{11}	2.13×10^{-8}	7.00×10^{11}	8.56×10^{-8}
7.50×10^{11}	2.55×10^{-9}	7.50×10^{11}	3.38×10^{-8}	7.50×10^{11}	1.25×10^{-7}
8.00×10^{11}	5.62×10^{-9}	8.00×10^{11}	4.97×10^{-8}	8.00×10^{11}	1.72×10^{-7}
8.50×10^{11}	1.10×10^{-8}	8.50×10^{11}	6.87×10^{-8}	8.50×10^{11}	2.26×10^{-7}
9.00×10^{11}	1.95×10^{-8}	9.00×10^{11}	9.08×10^{-8}	9.00×10^{11}	2.86×10^{-7}
9.50×10^{11}	3.21×10^{-8}	9.50×10^{11}	1.15×10^{-7}	9.50×10^{11}	3.51×10^{-7}
1.00×10^{12}	4.95×10^{-8}	1.00×10^{12}	1.42×10^{-7}	1.00×10^{12}	4.19×10^{-7}

Appendix C

Power emitted by the edge of a SC dipole ($L = 2.5$ cm)

a) $\lambda_2 = 150$ nm $\lambda_1 = 300$ nm detector 1		b) $\lambda_2 = 450$ nm $\lambda_1 = 650$ nm detector 2		c) $\lambda_2 = 350$ nm $\lambda_1 = 1100$ nm detector 2	
Proton energy (eV)	Total emitted power for 10^{14} p (W)	Proton energy (eV)	Total emitted power for 10^{14} p (W)	Proton energy (eV)	Total emitted power for 10^{14} p (W)
4.50×10^{11}	4.84×10^{-12}	4.50×10^{11}	2.39×10^{-10}	4.50×10^{11}	1.72×10^{-9}
5.00×10^{11}	2.50×10^{-11}	5.00×10^{11}	9.10×10^{-10}	5.00×10^{11}	6.14×10^{-9}
5.50×10^{11}	1.01×10^{-10}	5.50×10^{11}	2.93×10^{-9}	5.50×10^{11}	1.88×10^{-8}
6.00×10^{11}	3.42×10^{-10}	6.00×10^{11}	8.27×10^{-9}	6.00×10^{11}	5.16×10^{-8}
6.50×10^{11}	1.00×10^{-9}	6.50×10^{11}	2.11×10^{-8}	6.50×10^{11}	1.29×10^{-7}
7.00×10^{11}	2.63×10^{-9}	7.00×10^{11}	4.97×10^{-8}	7.00×10^{11}	2.98×10^{-7}
7.50×10^{11}	6.29×10^{-9}	7.50×10^{11}	1.09×10^{-7}	7.50×10^{11}	6.48×10^{-7}
8.00×10^{11}	1.40×10^{-8}	8.00×10^{11}	2.27×10^{-7}	8.00×10^{11}	1.34×10^{-6}
8.50×10^{11}	2.92×10^{-8}	8.50×10^{11}	4.49×10^{-7}	8.50×10^{11}	2.65×10^{-6}
9.00×10^{11}	5.77×10^{-8}	9.00×10^{11}	8.54×10^{-7}	9.00×10^{11}	5.03×10^{-6}
9.50×10^{11}	1.09×10^{-7}	9.50×10^{11}	1.57×10^{-6}	9.50×10^{11}	9.27×10^{-6}
1.00×10^{12}	1.98×10^{-7}	1.00×10^{12}	2.79×10^{-6}	1.00×10^{12}	1.66×10^{-5}

Appendix D

Monitor performance for 10^{14} p

E_{beam}	450 GeV			1 TeV			8 TeV		
Detector	Intensifier	Intensifier	Intensifier	Intensifier	CCD	CCD	Intensifier	CCD	CCD
λ [nm]	150–300	450–650	350–1100	150–300	450–650	350–1100	150–300	450–650	350–1100
σ_h [μm]	2501			1677			593		
σ_v [μm]	1250			839			297		
σ_{mh} [μm]	2506	2515	2524	1687	1699	1719	688	927	1016
σ_{mv} [μm]	1258	1260	1261	850	844	847	347	328	328
$E_{detector}$ [μJ/cm^2]	8×10^{-8}	2×10^{-5}	2×10^{-4}	1×10^{-2}	3×10^{-2}	0.1	0.16	5.3	12.4
V_{det}/V_{sat} [%]	0.4	100	100	100	16	60	100	76	80

σ_h is the horizontal r.m.s width
σ_v is the vertical r.m.s width
σ_{mh} is the horizontal measured r.m.s width
σ_{mv} is the vertical measured r.m.s width
$E_{detector}$ is the available energy density at the detector input
V_{det}/V_{sat} [%] is the ratio of the CCD output voltage to its saturation voltage after adjustment of the intensifier gain, if the latter is present.